Nuclear Instruments and Methods in Physics Research A242 (1986) 437–442
North-Holland, Amsterdam

THE FITTING OF SOLID STATE DETECTOR SPECTRA

W. WESTMEIER *

Institut für Kernchemie, Philipps-Universität, D-3350 Marburg, FRG

A procedure for background subtraction from semiconductor spectra and peak shape models for gamma-ray, conversion electron, and alpha particle peaks are described. The validity of the proposed algorithms is confirmed through calculations of sample spectra.

1. Introduction

With the widespread distribution of high-resolution semiconductor detectors, the assay of complex γ-ray, conversion electron, and alpha particle spectra has become feasible. The quantitative evaluation of peak areas in these spectra through summation of counts is simple, provided that one is concerned with singlet peaks sitting on a *known* background distribution. In the case that multiplet peaks are to be evaluated one has to know, in addition to the background distribution under the multiplet, an analytical peak shape description in order to apply fitting algorithms as published for example in refs. [1–7]. However, both master criteria, the background distribution as well as the peak shape parameterization of photon and particle peaks, up to now seem to be subject to approximations.

In this paper I want to present an analytical method for background calculation from the measured spectrum and peak shape descriptions for particle and photon peaks originating from physics-oriented modeling or well substantiated experience, respectively.

2. Background subtraction

When evaluating the areas of peaks in semiconductor spectra, one first has to consider the background (BGD) distribution under the peaks. It is obvious that the inclusion of all BGD counts to the peak area, i.e., the summation of counts from peak start to peak end, yields a too large area. Thus one has to separate the BGD distribution from each peak or multiplet prior to evaluation. This problem has first been surveyed by Pratt [8]. In a publication from Helmer et al. [6] a review of commonly used BGD shape functions is given. Fig. 1 shows some of these functions. Simple BGD recipes such as straight line representation are omitted in the plot.

The generation of a BGD distribution is physically linked to the full energy events in a spectrum via different types of interactions. Thus, apart from statistical effects, a given photopeak will be associated with a unique BGD distribution. This direct relationship is only dependent on performance characteristics of the detector. In order to reconstruct the BGD distribution from an experimentally determined sum of BGD and photopeak events an empirical model algorithm was developed [9].

For simplicity the algorithm is described for a singlet photopeak, but it is applicable to multiplets, too. A detailed inspection of the BGD shape shows that the distribution is almost constant in the immediate (and relevant) low energy vicinity of a peak. On the high energy side of the peak one finds BGD events as well which are produced by radiation whose photopeaks are situated at higher energies.

As a start one may use a schematic peak and BGD distribution as indicated in fig. 2. A photopeak in

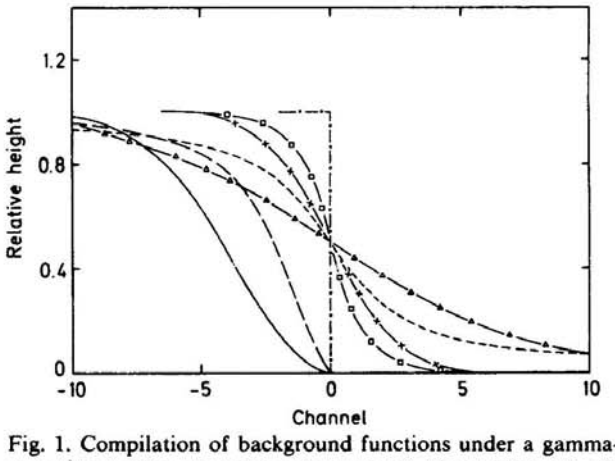

Fig. 1. Compilation of background functions under a gamma-ray peak positioned at channel number 0. Figure after ref. [6].

* Present address: Kernspektrometrie, Beratung & Software, Möllner Weg 5, D-3557 Ebsdorfergrund 2, FRG.

0168-9002/86/$03.50

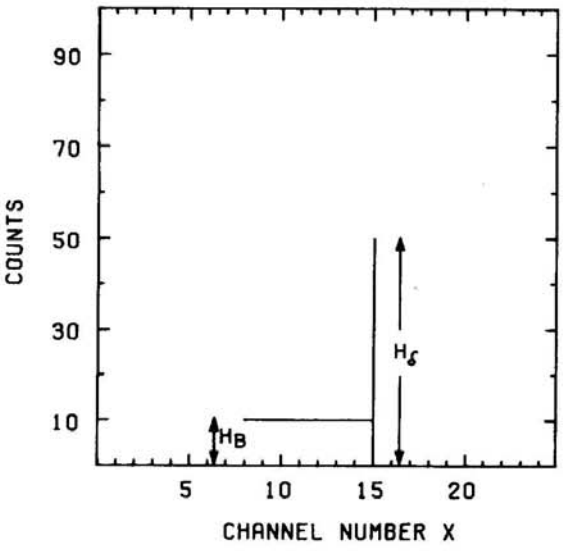

Fig. 2. Schematic representation of a peak δ-function and the constant background at lower energy.

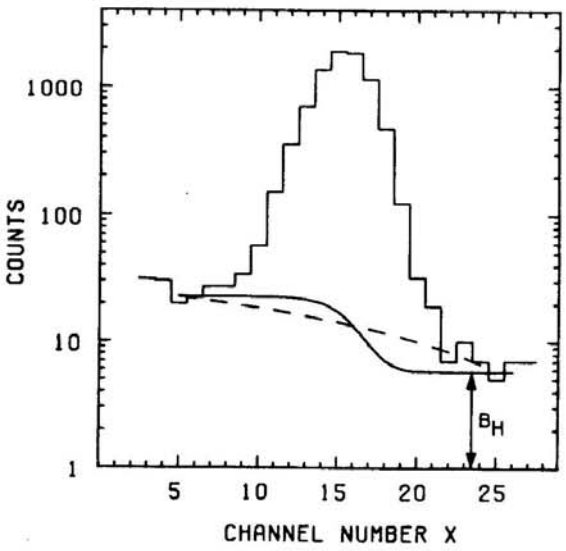

Fig. 3. Sum of a Gaussian cluster of δ-lines plus background shares. For details, see text.

channel 15 (δ-line) is associated with no BGD distribution in higher channel numbers and with a constant distribution below channel 15. The height of the low energy BGD function H_B relative to the height of the δ-line H_δ is an unknown constant:

$$H_B = \text{const.}\ H_\delta. \tag{1}$$

The term height is used as a synonym to number of counts per channel. The actually measured photopeak is not a δ-line but it rather has some Gaussian width. To a good approximation one may represent such a distribution as a cluster of one-channel wide δ-lines whose height distribution follows a Gaussian function. Each of these δ-lines is associated with a constant low energy BGD distribution according to eq. (1). For each channel x one may simply add up all contributions to gain the total number of counts Y, i.e.,

$$Y(x) = B_H + H_\delta(x) + \sum_{z=x}^{x_1} \text{const.}\ H_\delta(z), \tag{2}$$

where x_1 is the end channel of the current cluster of δ-lines above channel x (i.e., the next peak) and B_H is the BGD originating from peaks above x_1. Taking a constant value of 5.8 counts for B_H, an experimental BGD plus peak distribution is plotted in fig. 3 as a histogram. The full line under the peak shows the underlying distribution generated from eq. (2) but without the $H_\delta(x)$ summands. Thus, this full distribution corresponds to the required BGD.

In order to extract the BGD distribution from a measured spectrum one simply has to solve eq. (2) but without the $H_\delta(x)$ term for each individual channel x. As the BGD distribution before and after a peak can be found by smoothing the spectral counts distribution in these regions one only has to consider the region under a peak i.e., channels 5–25 in the example of fig. 3. The relevant part to be evaluated from eq. (2) is the summation term. This, however, requires the knowledge of the H_δ-line heights which are approximated by subtraction of a linear BGD function between channels 5 and 25 (dashed line in fig. 3) of the example peak. Starting from the top channel number 25, we now sum up the H_δ's, going in one channel steps down to channel 5. This integral distribution $I(x)$ is in effect the desired BGD distribution shape under the peak but without consideration of the unknown factor const. from the sum in eq. (2). The factor is gained by normalizing the start value of the integral ($I(25) = 0$) to the BGD height in channel 25 and the end value of the integral ($I(5) =$ sum of all H_δ values) to the BGD height in channel 5. $I(x)$ is the number of integrated counts up to channel x. Through the normalization of $I(25)$ to the BGD in channel 25 one evenly considers the term B_H in eq. (2). In this fashion one can directly generate a consistent BGD distribution from a measured spectrum without knowing any details about constituents in multiplets of overlapping peaks. One simply has to generate peak start and peak end positions for each singlet or multiplet peak and to perform the integration and normalization as described above. A systematic error, however, is inherent to the procedure through the approximation of the H_δ distribution which is gained by subtraction of a linear function rather than the correct BGD. As one generates only an approximate H_δ distribution which then is integrated, one obtains only approximate BGD distributions. As a consequence, the analyzed peak after BGD subtraction will yield a slightly low peak area. For a detector with a P/C ratio of 25/1, this error amounts

to less than 0.03%, and it decreases with increasing P/C values.

3. Peak shape description

From text book descriptions (see e.g. ref. [10]) it is clear that the center portions of photon, alpha particle, and conversion electron peaks are well described by Gaussian distributions. Any fitted peak function thus has the basic analytical form

$$Y_G(x) = \mathrm{HGT}/\exp\left((x - \mathrm{POS})^2 4\frac{\ln 2}{\mathrm{fwhm}^2}\right), \qquad (3)$$

where HGT is the height of the Gaussian (in counts), POS is the peak position (in channels), fwhm is the full width at half maximum, and $Y_G(x)$ is the height of the Gaussian in channel number x. This Gaussian is used for fitting the high energy flank of each peak because properly measured semiconductor detector spectra exhibit no high energy peak tailing. The approximations used for the description of low energy tails are described in the following.

3.1. Photon peak tailing

There are several functions presented in the literature which are used as approximate descriptions of the low energy tailing of photon peaks. None of these functions is based on theoretical arguments. Rather they are all empirical trial functions. An empirical tailing function successfully applied to the analysis of complex photon spectra in our laboratory as well as at other places has the form

$$G(x) = Y_G(x)\left(1 - \mathrm{CAPPA}(x - \mathrm{POS})^5\right),$$

$$\text{for } x < \mathrm{POS}, \qquad (4a)$$

where $G(x)$ is the height of the peak function in channel x, $Y_G(x)$ is the net height of the Gaussian function (eq. (3)) at channel x, POS is the peak position and CAPPA is a free fit parameter. Due to the high power of the $(x - \mathrm{POS})$ term this functional dependence allows for the generation of a long low energy tail. For positive values of $(x - \mathrm{POS})$ the peak function has the form of eq. (3) i.e., it is taken to be an undisturbed Gaussian

$$G(x) = Y_G(x), \qquad \text{for } x \geqq \mathrm{POS}. \qquad (4b)$$

There is no reference yet to this low energy tailing description nor is there any theoretical justification of the function from eq. (4a). The only reason why this function is used in preference over other low energy tailing functions for the analysis of photon peaks is the improved fitting ability. It would certainly be desirable to find the link between the functional description of eq. (4) and the physical occurrences.

3.2. Electron peak tailing

It has been tried to fit the low energy tailing distribution from singlet electron peaks in sample spectra with theoretical shapes expected from bremsstrahlung or backscattering. None of these nor the combination of both theoretically expected tailing contributions can account for the actually measured distribution and at the same time allow for the fitting with only a few parameters. Electron peak shapes as described by Damkjaer [11] could not be successfully applied to the fitting of sample spectra. A numerical inspection of electron peaks shows that at large distances from the peak position there is an exponential decrease of the tailing as is expected from absorption. It was therefore decided to trace back the exponential low energy tailing to its origin and to find a suitable description of the tailing shape. The procedure applied resembles in some respect the algorithm which is used for the generation of the BGD distribution from spectra.

The assumed "peak shape" of conversion electrons is a δ-function at some channel number. Due to absorptive processes between emission and registration, some fraction of the electrons may lose energy. The consequence encountered in the spectrum is an exponential low energy tailing to the δ-line which is schematically sketched in fig. 4. Such exponentially falling intensity distributions are found for all undisturbed absorptive processes which start from identical primary states and in which neither absorber gradients nor external influences play a role (see for example: Lambert–Beer's law). In the interaction of electrons (or alpha particles) with matter, major external influences such as changing charge states or the transition from the electronic to the nuclear stopping power regime can be neglected. There-

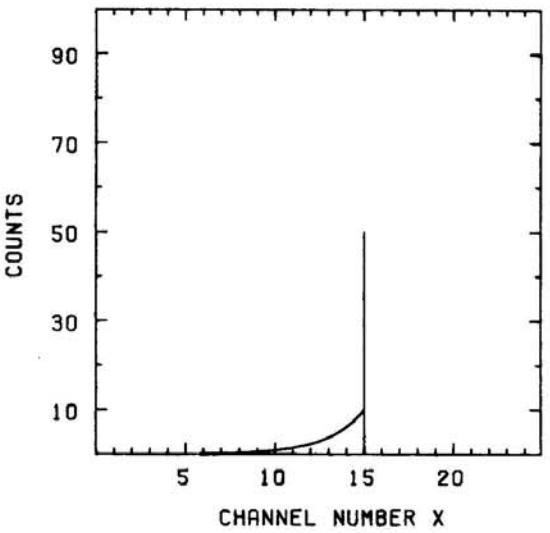

Fig. 4. Schematic representation of an electron peak as a δ-line with exponential low energy tailing.

fore one expects to find one characteristic exponential low energy absorption tail when electrons or alpha particles interact with matter on their path between emission and registration. In fig. 4 the intrinsic δ-function at channel POS = 15 with a height of HGT = 50 has an exponential low energy tail which starts at 0.2 $HGT_\delta (= H_1\ HGT_\delta)$ and which is described via the equation

$$Y_{tail}(x) = HGT_\delta\ H_1 \exp(D_1(x - POS)). \quad (5)$$

D_1 is 0.5 in the example. The real peak shape of conversion electrons, however, is a Gaussian distribution centered at channel 15. As energy dispersive spectra are measured in equally wide channel bins one may look at the Gaussian distribution as a cluster of δ-functions around channel 15 where each of the δ-functions contributes with its own exponential tailing fraction according to eq. (5). Thus, the measured contents of a particular channel x is the height of the Gaussian δ-function in x plus the sum of all tailing shares originating from δ-functions in channels above x. In fig. 5 the resulting spectral distribution is plotted for a peak generated with:

POS = 15 (channels),
HGT = 50 (counts),
fwhm = 3 (channels),
$H_1 = 0.2$ (in units of HGT),
$D_1 = 0.5$.

The second, smaller peak around channel 14 which merges with the sum peak at about channel 11 is the contribution originating from the exponential low energy tailing sums alone. This peak distribution which is calculated according to the simple and straightforward model presented above greatly resembles the actually measured peak shape in sample spectra and therefore an analytic function for the analysis of electron (and alpha particle) spectra is deviced on the basis of this model. The function fitted to the peaks is

$$E(x) = G(x) + \sum_{z=x+1}^{N} G(z)\ H_1 \exp(D_1(x - z)), \quad (6)$$

where $E(x)$ is the total number of counts in channel x for an electron or alpha peak, $G(x)$ and $G(z)$ are as defined in eq. (4) and N is taken to be POS + 1.5 fwhm. This limitation of the summing to tailing shares from δ-functions up to 1.5 times fwhm above the peak position seems justified as the missing part to the total Gaussian area then is below 0.01% and the concurrent missing tailing share is even much smaller.

Inasmuch as the interaction of alpha particles and heavy ions with matter greatly resembles the interaction of electrons with matter, the analytical function for the fitting of electron peaks is well or even better applicable for heavy particle spectra. However, even under the premise of well optimized setups one has to expect a more pronounced contribution of the absorptive tail to the actual peak shape.

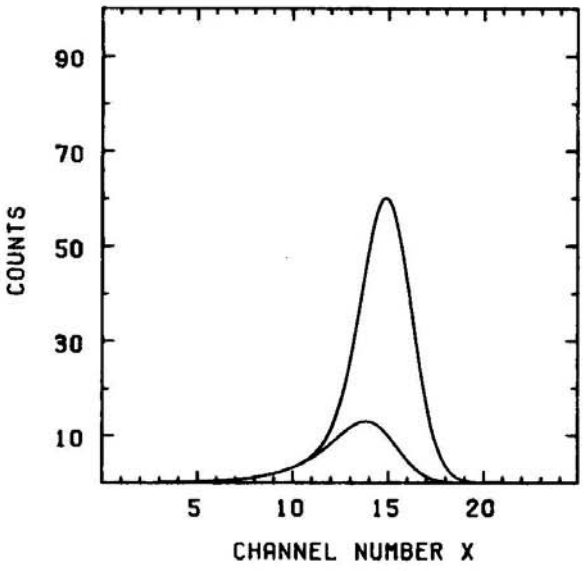

Fig. 5. Sum of a Gaussian distribution of δ-lines plus exponential tailing, and (below) the sum of tailing shares alone.

4. Examples of calculations

4.1. Gamma-ray spectra

As to demonstrate the good resolving power of the proposed algorithm for BGD subtraction and the photon peak shape, the reader is referred to refs. [9,12] where very complex gamma-ray spectra were analyzed. The agreement of calculated areas even for tiny peaks with literature values as well as the consistency of product cross sections which are calculated from the peak areas is very good.

4.2. Conversion electron spectra

A conversion electron spectrum from a thin ^{133}Ba source is analyzed. For the analysis (see fig. 6) the peak multiplet including the peaks around channels 191, 203, and 206 is chosen. These are a photon peak in channel 206 (81 keV γ) and the associated e_{M+N} and e_L lines in channels 203 and 191, respectively. As none of these peaks is an outstanding singlet, the three overlapping peaks are evaluated simultaneously in one region being defined from channel 178 to 214, inclusively. The major difficulty in the analysis of this multiplet lies in the strong overlapping of the e_{M+N} and γ-peaks around channel 204 which exhibit no clearly separated peak maxima and which have to be simultaneously analyzed using very different peak shape parameters.

In order to demonstrate the physical significance of calculated values, I want to compare the results with

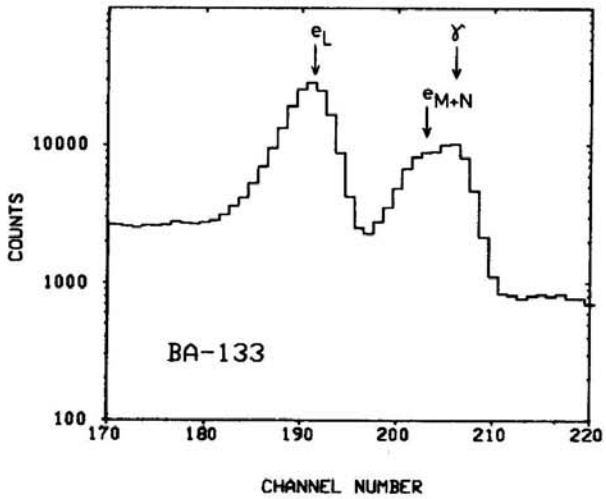

Fig. 6. Fraction of the conversion electron spectrum of ^{133}Ba.

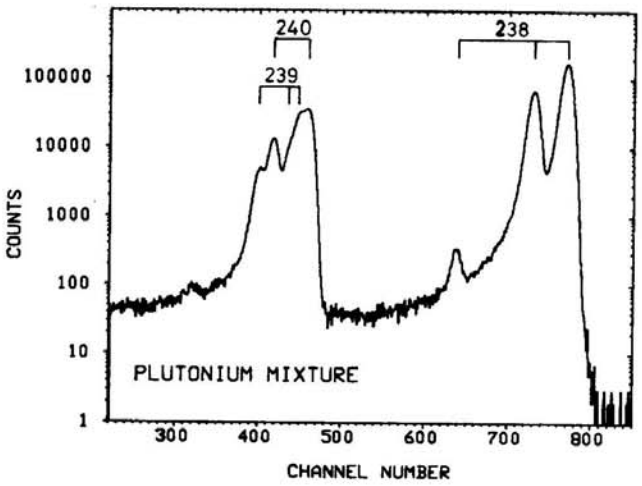

Fig. 7. Alpha particle spectrum from a source containing Pu isotopes from fuel reprocessing. The isotopic assignment of components is indicated above the spectrum.

literature values. The peaks analyzed are the e_L peak at channel (191.40 ± 0.02) with (147795 ± 1717) counts and the e_{M+N} peak at channel (203.10 ± 0.12) with (43035 ± 1499) counts which both originate from the γ-transition unconvertedly measured in channel (206.36 ± 0.08). Assuming equal detection efficiencies for both electron peaks, the intensity ratio I_{e_L}/I_{M+N} is calculated and compared to literature data. The calculated intensity ratio was (3.43 ± 0.13), while the ratio of Henneke [13] was (3.6 ± 0.4) and that of Henry [14] was (3.88 ± 0.82).

For the energy cross check we may equate the difference in peak positions between the photon peak and the e_L peak to the L_1 X-ray atomic level of cesium [15] (ΔE = (5714.3 ± 0.3) eV) and calculate from the M_1 X-ray atomic energy level (ΔE = (1217.1 ± 0.4) eV) that the e_{M+N} peak should be situated 3.19 channels below the photon peak. The difference calculated here amounts to (3.26 ± 0.14) channels which is incorrect by (0.07 ± 0.14) channels or (26 ± 53) eV. Considering the complete overlap of the photon and e_{M+N} peaks, this resolution with respect to peak positions and intensities is deemed to be excellent. It should be noted that the above results were obtained without fixing any peakshape parameter and through simultaneous use of different peak shape model descriptions. The good results of peak analysis are strongly supportive of the models employed for background subtraction and peak shape parameterization.

4.3. Alpha particle spectra

An alpha particle spectrum (see fig. 7) from a vacuum evaporated source of a solution containing plutonium isotopes ^{238}Pu through ^{242}Pu is evaluated. The sample was originally used for intercomparison purposes in an interlaboratory experiment [16] dealing with the high precision determination of Pu isotopes in solutions from reprocessing plants. In the following, the results of the analysis of the major ^{238}Pu peaks as well as of the $^{239/240}$Pu multiplet will be shown. Of special interest is the comparison of literature data with calculated values for the $^{238/239/240}$Pu peaks. In table 1 are listed the peak intensities as given in the literature [17] and the calculated values of this work. The contributions of minor intensities for ^{238}Pu (~ 0.0003%), ^{239}Pu (~ 0.1019%) and ^{240}Pu (~ 0.072%) are neglected in the analysis, assuming that the analyzed peaks constitute 100% of the α-intensity for each isotope.

Apparently the resolution of the α_0 and α_1 peaks of ^{239}Pu which both are buried in the low energy flank of the dominating α_0 peak of ^{240}Pu is incomplete. However, adding the calculated intensities of the α_0 and α_1 peaks of ^{239}Pu one gets an intensity of $I_{\alpha_0+\alpha_1}$ = (88.7 ± 3.9)% which is in good agreement with the literature value of (88.4 ± 0.7)%, i.e., the ^{239}Pu intensity is well resolved from the ^{240}Pu peak.

In order to test the consistency of calculated peak

Table 1
Comparison of calculated α-intensities with literature values

Nuclide	α-transition	I_α, literature (%)	I_α, this work (%)
^{238}Pu	α_0	71.6 ±0.6	71.9 ±1.3
	α_1	28.3 ±0.6	28.0 ±0.5
	α_2	0.10±0.03	0.13±0.01
^{239}Pu	α_0	73.3 ±0.7	69.7 ±3.5
	α_1	15.1 ±0.2	19.0 ±1.8
	α_2	11.5 ±0.2	11.3 ±0.9
^{240}Pu	α_0	73.5 ±0.4	72.5 ±2.7
	α_1	26.4 ±0.2	27.5 ±1.2

Table 2
Comparison of the isotopic contents of a plutonium reprocessing sample determined via mass- and alpha-spectrometry.

Isotope	Mass spectrometer [16] (%)	This work (%)
^{238}Pu	1.848	1.874 ± 0.050
^{239}Pu	71.225	71.713 ± 2.909
^{240}Pu	26.926	26.413 ± 0.883

areas one may convert them into unnormalized atomic contents of the sample and compare the resulting atomic percentages with values obtained through two independent mass spectrometric surveys [16] of the same sample. The resulting percentages are listed in table 2.

Acknowledgments

I want to thank the Central Bureau for Nuclear Measurements (CBNM, Geel, Belgium) and the Fachinformationszentrum Energie, Physik, Mathematik GmbH in Karlsruhe who enabled me to do this survey. Special gratitude is due to Prof. P. Patzelt for his hospitality and support.

References

[1] M.A. Mariscotti, Nucl. Instr. and Meth. 50 (1967) 309.
[2] J.T. Routti and S.G. Prussin, Nucl. Instr. and Meth. 72 (1969) 125.
[3] R. Gunnink and J.B. Niday, Report UCRL-51061, Vol. 1, Lawrence Livermore Laboratory (1972).
[4] M. Hillman, Nucl. Instr. and Meth. 135 (1976) 363.
[5] U. Abbondanno, A. Boiti, F. Demanins and M.R. Malisan, Nucl. Instr. and Meth. 148 (1978) 577.
[6] R.G. Helmer and M.A. Lee, Nucl. Instr. and Meth. 178 (1980) 499.
[7] P. Urwank, Nucl. Instr. and Meth. 203 (1982) 329.
[8] T.A.E.C. Pratt, Nucl. Instr. and Meth. 99 (1972) 205.
[9] W. Westmeier, Nucl. Instr. and Meth. 180 (1981) 205.
[10] G.F. Knoll, Radiation Detection and Measurement (Wiley, New York, 1979).
[11] A. Damkjaer, Nucl. Instr. and Meth. 200 (1982) 377.
[12] R.A. Esterlund, W. Westmeier, U. Reus, A.M. Habbestad Wätzig and P. Patzelt, Nucl. Phys. A435 (1985) 597.
[13] H.J. Hennecke, J.C. Manthuruthil, O. Bergman and C.R. Cothern, Phys. Rev. 159 (1967) 955.
[14] E.A. Henry, Nucl. Data Sheets 11 (1974) 495.
[15] CRC Handbook of Chemistry and Physics, 56th ed., ed., R.C. Weast (CRC Press, Cleveland, Ohio, 1975).
[16] G. Bortels et al., Report No. KfK 2862/EUR6402e, Kernforschungszentrum Karlsruhe (1979).
[17] Proposed Recommended List of Heavy Element Radionuclide Decay Data, IAEA Report INDC(NDS)-149/NE, ed., A. Lorenz (IAEA, Wien, 1983).